ACS APPLIED MATERIALS & INTERFACES

Research Article

www.acsami.org

# Nanostructured Aqueous Lithium-Ion Conductors Formed by the Self-Assembly of Imidazolium-Type Zwitterions

Xinpei Gao, Fei Lu, Lijuan Shi, Han Jia, Hejun Gao, and Liqiang Zheng*

Key Laboratory of Colloid and Interface Chemistry, Shandong University, Ministry of Education, Jinan 250100, P. R. China

Supporting Information

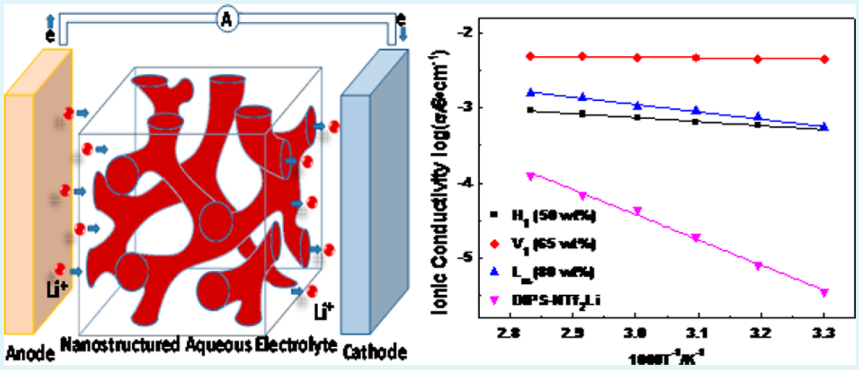


**ABSTRACT:** In the present study, we have synthesized a room-temperature ionic liquid by mixing imidazolium-type zwitterions with lithium bis(trifluoromethanesulfonyl)imide. We constructed nanostructured aqueous lithium-ion conductors having hexagonal, lamellar, and bicontinuous cubic structures by the self-assembly of this amphiphilic ionic liquid. These nanostructured lithium-ion conductors exhibited an assembled-structure dependent lithium-ion conduction behavior. The introduction of highly ordered and well-defined liquid crystal structures into room-temperature ionic liquid radically changes the conduction mechanism from diffusion to hopping.

**KEYWORDS:** *ionic liquid crystals, zwitterions, ionic liquids, self-assembly, electrolyte*

## INTRODUCTION

The rapid growth of the global economy and population arise a fast-growing demand for electrical energy.[1] There is a strong need for renewable energy such as solar, wind, and tide energy, as well as safe and reliable energy storage systems.[2] Aqueous rechargeable lithium batteries (ARLBs), which use aqueous electrolytes and lithium intercalation compounds as electrode(s) based on redox reactions, were invented in 1994 and have attracted wide attention as a promising system because of their low capital investment, high reliability, and good safety.[3,4] Recent breakthroughs clearly showed that ARLBs can exhibit impressive cycling performance and superfast charge performance.[5−7] All the previous studies about ARLBs were confined to improving the performance of the electrode materials.[8−10] Aqueous electrolytes have higher conductivity, but solid or gel electrolytes are preferred because aqueous electrolytes can leak and have poorer fabrication properties.[11,12] The introduction of nanostructured ionic liquid crystals (ILCs) was a new approach to improve these defects.[13] Meanwhile, the safety issues arising from the toxic and flammable organic electrolyte are also avoided.

ILCs are a class of liquid crystalline compounds that are composed only of ionic species, which are interesting candidates for specific ion transportation. ILCs can be considered as materials that combine the properties of liquid crystals (LCs) and ionic liquids (ILs).[14] ILs have been considered as competitive solvents or electrolytes because of their unique properties such as low melting temperature, flame retardancy, negligible vapor pressure, and high ionic conductivity.[15,16] LCs have attracted increasing attention as functional soft materials because of their highly ordered and well-defined self-assembly structure.[17] Taking all of this into account, we believe that a suitable combination of the ILs and the LCs is a promising candidate for a novel nanostructured aqueous electrolyte that exhibits high lithium-ion conductivity while avoiding the defects of liquid electrolytes.

There are a limited number of reports on the application of ILC type ion-conduction materials. Hikmet and co-workers studied lithium-ion conducting gel electrolytes containing low molecular mass organic solvents.[18] Gin and co-workers have achieved 3D nanostructured carbonate-based LC electrolytes using lyotropic LC $Cub_{bi}$ systems.[19] Ohno's group developed several ion conduction materials based on the principle of self-organization of thermotropic LCs.[20−22] However, to the best of our knowledge, no study has been reported on the preparation of nanostructured aqueous lithium-ion conducting electrolytes.

**Received:** September 30, 2013
**Accepted:** November 15, 2013
**Published:** November 15, 2013

   dx.doi.org/10.1021/am404288x | *ACS Appl. Mater. Interfaces* 2013, 5, 13312−13317

Our group has previously reported several ILC systems using imidazolium or pyrrolidinium ILs.[23−25] But in these kinds of ILCs, the specific ion transportation was hindered by the migration of counterions. To overcome the disadvantages of conventional ILCs, such as their low target ion transport number and lack of selectivity, researchers have proposed zwitterions with covalently bonded cations and anions as a candidate for specific ion transportation.[26]

In the present study, we constructed nanostructured aqueous lithium-ion conductors having hexagonal, lamellar and bicontinuous cubic structures using imidazolium-based zwitterions with lithium bis(trifluoromethanesulfonyl)imide. The microstructures and phase behaviors of the obtained ILCs were studied by polarized optical microscope (POM), small-angle X-ray scatting (SAXS) and rheological measurement. The ionic conductivities of ILCs were investigated by alternating current impedance method. It is the first attempt to improve the performance of aqueous electrolyte used in ARLBs by the introduction of the ILCs. The topological structure constructed in ILCs radically changes the conduction mechanism from diffusion to hopping. We expect this work may shed light on the potential of nanostructured aqueous lithium-ion conducting ILCs electrolytes in practical applications.

## EXPERIMENTAL SECTION

**Materials.** Lithium bis(trifluoromethanesulfonyl)imide ($NTf_2Li$, 98%), 1-bromododecane (98%), 1,3-propanesultone(99%), and imidazole (99%) were purchased from J&K Scientific Ltd. Sodium hydroxide, acetone and tetrahydrofuran were purchased from Shanghai Chemical Co. All the above materials were used without further purification. Deionized water was used through the experiment.

**Synthesis of 1-Dodecylimidazole.** The 1-dodecylimidazole was synthesized according to the procedures previously reported.[27] 1-bromododecane (24.92 g, 100 mmol) in tetrahydrofuran was added dropwise into a solution of imidazole (6.81 g, 100 mmol) in NaOH (50%) solution (8.8 g, 110 mmol). The mixture was refluxed for 3 days. Then tetrahydrofuran was removed by a rotary evaporator. The residue was extracted with dichloromethane/water three times. The produced 1-dodecylimidazole was dried under a vacuum at room temperature to obtain a clear yellow oil (17.96 g, 76% yield).

**Synthesis of 3-(1-Dodecyl-3-imidazolio)propanesulfonate-(DIPS).** 1-Dodecylimidazole (15.8 g, 0.067 mol) was dissolved in 80 mL of acetone. Then an equimolar amount of 1,3-propanesultone (8.2 g, 0.067 mol) in acetone (40 mL) was slowly added to the solution at 0 °C under a nitrogen atmosphere. The reaction mixture was then stirred for 5 days at room temperature. After the reaction, the solution was filtered and the zwitterionic salt (DIPS) was twice purified with acetone. The DIPS was dried under a vacuum at room temperature and a white powder was obtained (14.76 g, 61% yield). The purity of the product was ascertained by the $^1$H NMR (300 MHz) in DMSO.[28] $\delta$ (relative to TMS): 9.177 (1H, s), 7.800 (1H, t, $J$ = 1.8 Hz), 7.780 (1H, t, $J$ = 1.8 Hz), 4.298 (t, 2H, $J$ = 7.2 Hz), 4.143 (2H, t, $J$ = 7.2 Hz), 2.392 (2H, t, $J$ = 7.2 Hz), 2.088 (2H, quint, $J$ = 7.2 Hz), 1.804 (2H, m), 1.239 (18 H, m), 0.85 (t, 3H, $J$ = 6.6 Hz).

**Preparation of Samples.** The DIPS-$NTf_2Li$ aqueous mixture samples were prepared by weighing all components at designed compositions (in weight percent, wt%). DIPS and $NTf_2Li$ were mixed in an equimolar ratio, and the water content varied from 20 to 80 wt %. The mixtures were homogenized and equilibrated by repeated vortex mixing and centrifugation. Then the samples were kept at 25 °C for at least 1 month before further examination. During this incubation process, all the samples were sealed in stoppered glass vials to avoid evaporation.

**Characterization.** A polarized optical microscope (Olympus BX51p) equipped with cooled CCD (Evolution MP5.1RTV, Q-imaging, Canada) was used to observe textures of the LC phase. The temperature was controlled at 25 °C with a Linkam THSME600 liquid crystal freezing and heating stage system with a TP94 temperature controller (Linkam Scientific Instrument Ltd., UK). Small-angle X-ray scattering (SAXS) measurements were carried out on the SAXSess mc$^2$ X-ray scattering system (Anton Paar). SAXS measurement was performed with Cu K$\alpha$ radiation operating at 2 kW (50 kV and 40 mA). The distance between the sample and detector was about 264.5 mm and the wavelength of X-rays was 1.542 Å. The exposure time was 600 s for all samples. Rheological measurements were performed with a HAAKE RS 75 rheometer. A cone−plate sensor with a 20 mm diameter and a 1u cone angle was used. The cone−plate distance was adjusted to 52 mm for all measurements. The temperature was kept at 25 °C. The ionic conductivities of the ILCs were investigated by the alternating current impedance method in the frequency range of 100 mHz to 10 MHz with 0.01 mV oscillating voltage using an ITO cell consisting of a pair of ITO glass electrodes and a Teflon spacer.

## RESULTS AND DISCUSSION

The chemical structure of the molecule designed in the present study is shown in Scheme 1a. The amphiphilic zwitterion 3-(1-dodecyl-3-imidazolio)propanesulfonate (DIPS) consists of two incompatible parts: a hydrophilic imidazole zwitterionic part and a hydrophobic alkyl chain part. DIPS is a hydrophobic salt with high melting point. A room-temperature hydrophilic IL was obtained by evaporation of a methanol solution of equimolar DIPS and lithium bis(trifluoromethanesulfonyl)-imide ($NTf_2Li$). The decrease in the melting point and increase in the solubility are explained by the hard−soft acid−base principle.[29] The preferential interactions between the soft imidazole cation and the soft $NTf_2$ anion plays the key role in the formation of DIPS-$NTf_2Li$ IL.[30] It is generally accepted that nanosegregation between the hydrophobic alkyl chain part and hydrophilic zwitterion/$NTf_2Li$ part determines the formation of topological structures in ILCs.[26] To promote the nano-segregation between hydrophobic and hydrophilic parts, an appropriate amount of water was added to the DIPS-$NTf_2Li$ IL. The temperature−composition phase diagram of DIPS-$NTf_2Li$ aqueous mixture is shown in Figure 1a, together with the corresponding POM images. As shown in the phase diagram, the single-phase region consists of a wormlike micelle solution phase ($W_m$), an anisotropic hexagonal phase ($H_1$), an isotropic Ia3d bicontinuous cubic phase ($V_1$), and an anisotropic lamellar phase ($L_\alpha$). With an increase in DIPS-$NTf_2Li$ content, the phase transition of $W_m \rightarrow H_1 \rightarrow V_1 \rightarrow L_\alpha$ was confirmed.

**Scheme 1. (a) Molecular Structure of Amphiphilic Zwitterions 3-(1-Dodecyl-3-imidazolio)propanesulfonate (DIPS); (b) Ion Structure of Lithium Bis(trifluoromethanesulfonyl)imide ($NTf_2Li$)**

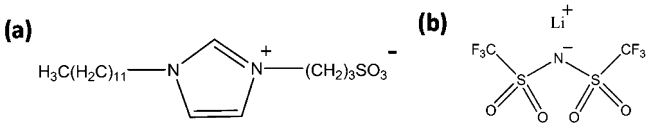


Figure 2 shows the SAXS patterns of the DIPS-$NTf_2Li$ aqueous mixture system with increasing DIPS-$NTf_2Li$ content collected at 25 °C. At low DIPS-$NTf_2Li$ content (20 wt %), two broad scattering peaks were observed in the SAXS pattern. Further rheological measurements demonstrated that the viscoelastic behavior of this sample closely follow the Maxwell behavior. As shown in Figure 3a, the solution shows a viscous behavior at the low frequency region ($G'' > G'$); as frequency increases, $G'$ and $G''$ increase and cross at a frequency $\omega_{co}$, above which the solution shows a elastic behavior ($G' > G''$).

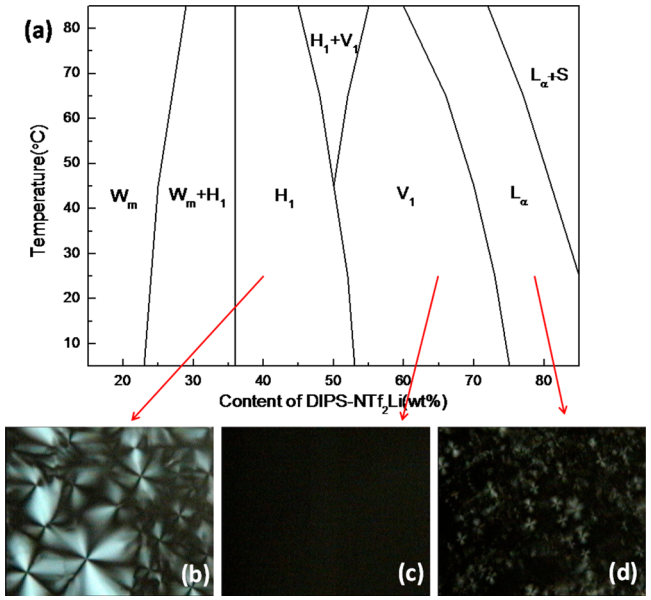


**Figure 1.** (a) Phase diagram of the DIPS-$NTf_2Li$ aqueous mixture. The meaning of the symbols labeled in the diagram is as follows: $W_m$ (worm-like micelle solution), $H_1$ (hexagonal phase), $V_1$ (Ia3d bicontinuous cubic phase), $L_\alpha$ (lamellar phase). (b–d) POM images of 40, 65, and 80 wt % samples collected at 25 °C.

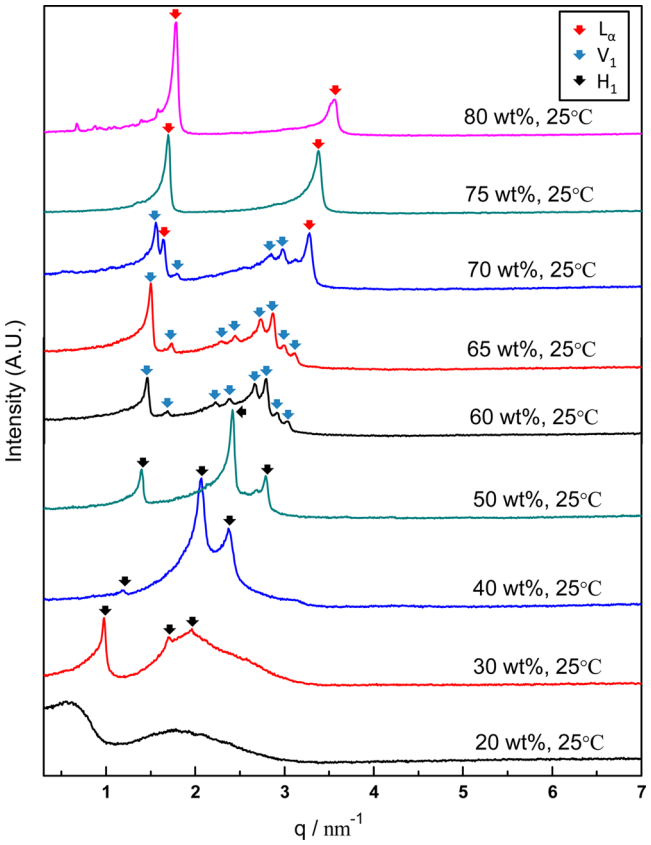


**Figure 2.** SAXS patterns of the DIPS-$NTf_2Li$ aqueous mixture system with increasing DIPS-$NTf_2Li$ content collected at 25 °C. Down arrows in different colors correspond to scattering peaks of different phases.

Figure 3b shows the Cole–Cole plot from the data presented in Figure 3a. The experimental points closely follow the Maxwell behavior at low frequencies, whereas at high frequencies, deviations from the semicircular Cole–Cole plots occur, showing the nonreptative high-frequency effects. All of these rheological patterns are in good accordance with the typical rheological behavior of wormlike micelles, indicating the existence of a concentrated wormlike micelle solution phase.[31,32] As the content of DIPS-$NTf_2Li$ increased to 30 wt %, three scattering peaks corresponding to hexagonal columnar structure and the broad peak observed in the $W_m$ phase appear simultaneously, indicating the possible coexistence of a concentrated worm-like micelle and a hexagonal columnar structure.[33] When the DIPS-$NTf_2Li$ content increased to 40 and 50 wt %, only three scattering peaks were observed. The ratio of these three peaks is $1:\sqrt{3}:2$, which are assigned to be the (100), (110), and (200) reflection of the hexagonal columnar structure. The fanlike texture shown in Figure 1b (40 wt %) is the typical character of the $H_1$ phase. An isotropic $V_1$ phase is found when the DIPS-$NTf_2Li$ content is between 60 and 70 wt %. The POM images shown in Figure 1c (65 wt %) displays only the background. Its SAXS pattern has eight scattering peaks with relative ratios of $\sqrt{3}:\sqrt{4}:\sqrt{7}:\sqrt{8}:\sqrt{10}:\sqrt{11}:\sqrt{12}:\sqrt{13}$, which can be indexed as the (211), (220), (321), (400), (420), (332), (422), and (510) reflections of a cubic structure with *Ia*3*d* symmetry.[34] As the content of DIPS-$NTf_2Li$ increased to 70 wt %, a phase transition from the $V_1$ phase to the $L_\alpha$ phase was observed. The SAXS pattern of this sample consists of two group of scattering peaks. The scattering peaks (marked with blue arrow) with relative ratios of $\sqrt{3}:\sqrt{4}:\sqrt{10}:\sqrt{11}$: were assigned to the (211), (220), (420), and (332) reflections of the Ia3d structure of the $V_1$ phase, while the scattering peaks (marked with red arrow) with relative ratios of 1:2 were assigned to the (100) and (200) reflections of the lamellar structure of the $L_\alpha$ phase. With a further increase in DIPS-$NTf_2Li$ content, the *Ia*3*d* structure disappeared, and the SAXS patterns of 75 and 80 wt % gave only the reflections of the lamellar structure. The crossed texture shown in Figure 1d is the typical texture for the $L_\alpha$ phase.

The phase behavior of DIPS-$NTf_2Li$ aqueous mixture system depends on not only the water content, but also the temperature. Figure 4a, b and c show the SAXS patterns of the DIPS-$NTf_2Li$ aqueous mixture in $H_1$, $V_1$ and $L_\alpha$ phases varying from 5 to 85 °C, respectively. For instance, the SAXS patterns of 50 wt % gave only reflections of the hexagonal columnar structure below 45 °C. When the temperature increased from 45 to 85 °C, the scattering peak assigned to the (110) reflection of hexagonal columnar structure disappeared gradually while the reflections of cubic structure with Ia3d symmetry was observed, demonstrating the coexistence of the $H_1$ phase and $V_1$ phase. In the SAXS patterns of 65 wt %, a phase transition from the $V_1$ phase to the $L_\alpha$ phase was observed when the temperature above 65 °C. In the SAXS pattern of 75 wt % collected at 85 °C, disorder scattering peaks were observed in the small angle region. We believe that these disorder scattering peaks at high temperature region were caused by the undissolved solid DIPS or $NTf_2Li$ due to the high concentration. Figure 4d, e and f show the dynamic viscoelastic behavior for the representative samples of $H_1$ phase (d), $V_1$ phase (e) and $L_\alpha$ phase (f) constructed in the DIPS-$NTf_2Li$ aqueous mixture system. In the experimental frequency region, all the samples show an elastic behavior ($G'>G''$). All of the samples behave as shear-thinning fluids, and the viscosities of the bicontinuous cubic phase are much higher than the viscosities of the hexagonal phases and lamellar phases. Thus,

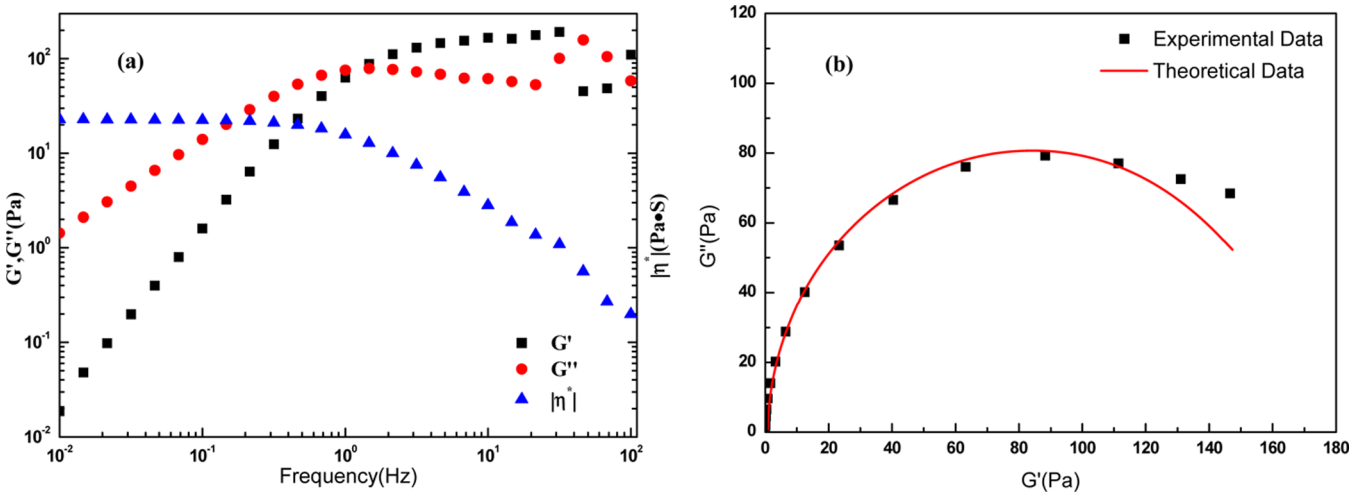


**Figure 3.** (a) Storage modulus $G'$, loss modulus $G''$, and complex viscosity modulus versus the frequency of the wormlike micelle solution phase (20 wt %) at 25 °C; (b) cole−cole plots of the wormlike micelle solution phase.

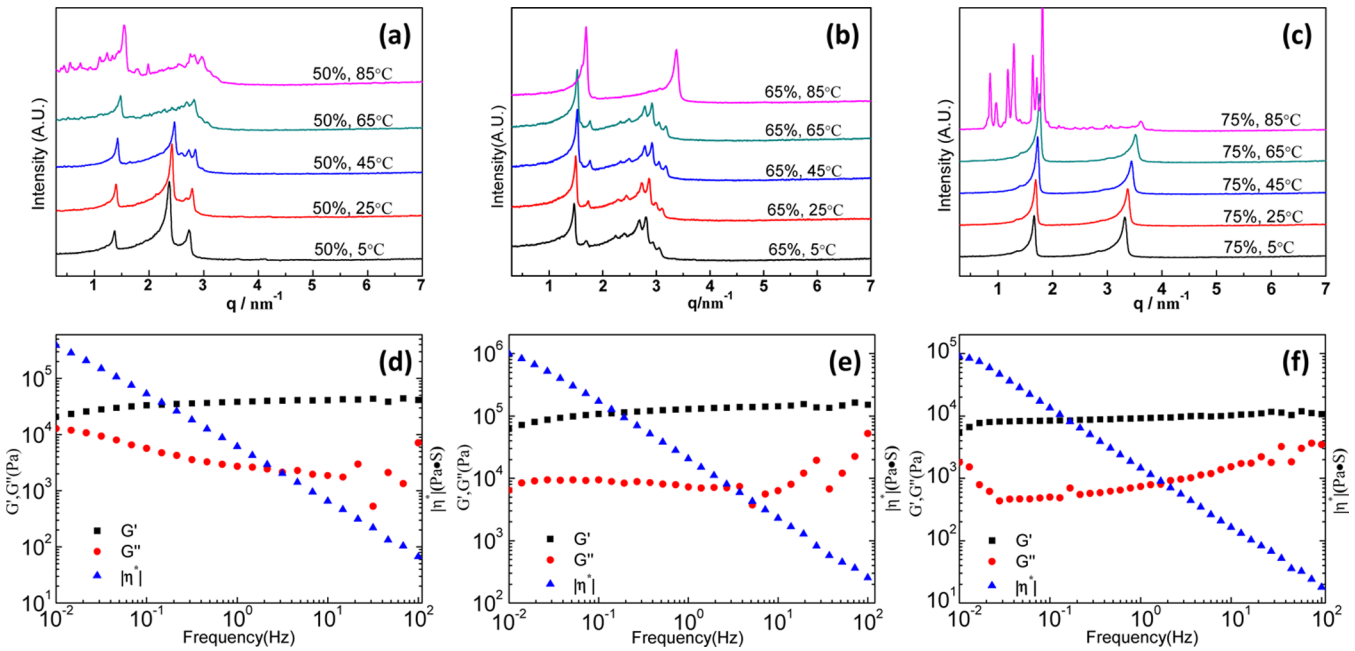


**Figure 4.** (a−c) SAXS spectra of 50, 65, and 75 wt % sample with the increasing temperature; (d−f) are oscillation shear behavior of 50 wt % sample in hexagonal phase, 65 wt % sample in bicontinuous cubic phase, and 75 wt % sample in lamellar phase at 25 °C.

**Table 1. Structural Parameters for the Liquid Crystalline Phases in the DIPS-$NTf_2Li$ Aqueous Mixture System**[a]

| Phase | Sample (wt%) | DIPS (wt%) | $NTf_2Li$ (wt%) | $H_2O$ (wt%) | $\Phi_L$ | $a_0$ (nm) | $r_H$ (nm) | $d_L$ (nm) | 2L (nm) | $d_W$ (nm) |
|---|---|---|---|---|---|---|---|---|---|---|
| | 30 | 16.6 | 13.2 | 70.2 | 0.1061 | 7.4233 | 1.2693 | | | 4.8847 |
| $H_1$ | 40 | 22.1 | 17.8 | 60.1 | 0.1458 | 6.1035 | 1.2237 | | | 3.6560 |
| | 50 | 27.7 | 21.9 | 50.4 | 0.1876 | 5.2068 | 1.1840 | | | 2.8387 |
| | 60 | 33.1 | 26.7 | 40.2 | 0.2319 | 10.5458 | | | 0.7974 | 2.2167 |
| $V_1$ | 65 | 36.2 | 28.9 | 34.9 | 0.2571 | 10.4513 | | | 0.8778 | 2.1754 |
| | 70 | 38.6 | 30.0 | 31.4 | 0.2768 | 9.8759 | | | 0.8944 | 2.0020 |
| $L_\alpha$ | 75 | 41.9 | 33.5 | 24.6 | 0.3079 | 3.7168 | | 1.1442 | | 2.5726 |
| | 80 | 44.7 | 35.8 | 19.5 | 0.3340 | 3.5372 | | 1.1816 | | 2.3556 |

[a] $\varphi_L$ is the volume fraction of the hydrophobic long alkyl chain part; $a_0$ is the lattice parameters of the liquid crystalline phases; $r_H$ is the radius of cylinder unit in the hexagonal structure; $2L$ is the hydrophobic part length in the $Ia3d$ bicontinuous cubic structure; $d_L$ is the thickness of hydrophobic domain in the lamellar structure; $d_W$ is the thickness of the water channel of the liquid crystalline phases.

the samples in bicontinuous cubic phase can be considered as "hard gel" with better fabrication properties, which may be used as electrolytes for aqueous rechargeable lithium batteries in future.

The SAXS characterization of the LC phase is based on the long-range order in the LC state, and the relevant structural parameters of the different types of LC phases can be deduced from the SAXS pattern.[23] All of the parameters calculated from the SAXS results were obtained according to the equations and theory shown in the Supporting Information, and the values are listed in Table 1. It is clear that the positions of the first peak shifts right with increasing concentration of DIPS-$NTf_2Li$, which means that the lattice parameter $a_0$ decreases with the increase in DIPS-$NTf_2Li$ concentration. In the $H_1$ phase, as the DIPS-$NTf_2Li$ content increases, both the structural parameters of the hydrophobic part ($r_H$) and the hydrophilic part ($d_W$) decrease. In other words, the cylinderlike aggregates pack more densely because of the fact that the hydrophobic chain of DIPS shrinks more in the hexagonal region with a higher concentration of DIPS-$NTf_2Li$. However, a different tendency was observed in $V_1$ and $L_\alpha$ phases. The size of the hydrophobic part ($2L$, $d_L$) becomes larger with an increasing amount of DIPS-$NTf_2Li$, whereas the water layer ($d_W$) becomes thinner. This result suggests that at higher DIPS-$NTf_2Li$ concentration, the hydrophobic chain of DIPS molecules cannot further shrink and the distance between the soft imidazole cation and the soft $NTf_2$ anion was compressed. As a consequence, the mean area of surfactant head groups is decreased, which ultimately increases the molecular packing parameter and induces the phase transition.

The phase behavior of the DIPS-$NTf_2Li$ aqueous mixture system was taken as a guideline for the study of lithium-ion conduction behavior. We expect that the study of the microsturcture in the liquid-crystalline phase can help us better understand the lithium-ion conduction mechanism in the system. To study the lithium-ion conduction behavior in the DIPS-$NTf_2Li$ aqueous mixture system, we measured the ionic conductivities of the mixtures by an alternating current impedance method. Figure 5 shows the Arrhenius plots of ionic conductivity of the DIPS-$NTf_2Li$ aqueous mixture in different liquid crystal phases and DIPS-$NTf_2Li$ mixture without water during the heating process. It is noteworthy that the addition of water significantly enhances the ionic conductivity. The ionic conductivity of the sample with 65 wt % DIPS-$NTf_2Li$ in the $V_1$ phase is $4.54 \times 10^{-3}$ S $cm^{-1}$ at 30 °C, approximately 1000 times higher than that of the DIPS-$NTf_2Li$ mixture without water. The ionic conductivities of the sample with higher water content in the $H_1$ phase and the sample with lower water content in the $L_\alpha$ phase are almost the same at 30 °C, approximately 150 times higher than that of the DIPS-$NTf_2Li$ mixture without water. This interesting phenomenon indicates that the microstructure formed in the liquid crystalline phase rather than the water content plays the chief role for efficient lithium-ion conduction in the system. We infer that the mixtures in $H_1$ and $L_\alpha$ phases can form low-dimensional hydrophilic channels between the columns or the layered structures, which act as lithium-ion conductive pathways.[35] But these hydrophilic channels in $H_1$ and $L_\alpha$ phases are not continuous on the macroscopic scale. While in the bicontinuous cubic phase, 3D continuous hydrophilic channels can provide a macroscopically continuous lithium-ion conductive pathway even without any orientation control because of their 3D periodical topological structure.[36] The schematic

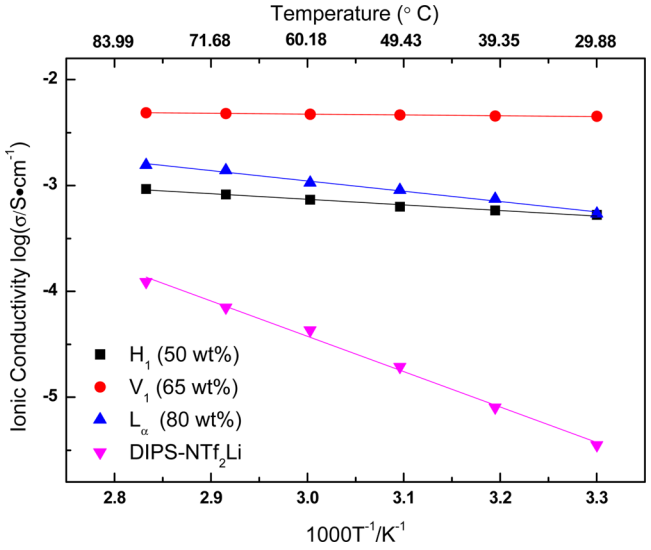


**Figure 5.** Arrhenius plots of ionic conductivity of the DIPS-$NTf_2Li$/$H_2O$ mixture in different liquid crystal phases: sample with 50 wt % DIPS-$NTf_2Li$ in $H_1$ phase (black squares); sample with 65 wt % DIPS-$NTf_2Li$ in $V_1$ phase (red circles); sample with 80 wt % DIPS-$NTf_2Li$ in $L_\alpha$ phase (blue triangles); and DIPS-$NTf_2Li$ mixture without water (pink triangles).

illustration of *Ia*3*d* bicontinuous cubic structure is shown in Scheme 2. The hydrophilic zwitterion/$NTf_2Li$ part forms the 3D continuous ionophilic layers as pathways inducing the hopping conduction of lithium ions.

**Scheme 2. Schematic Illustration of *Ia*3*d* Bicontinuous Cubic Structure; Red and the Blue Parts Represent the Hydrophilic Imidazole Zwitterionic Headgroup and the Hydrophobic Alkyl Chain, Respectively**

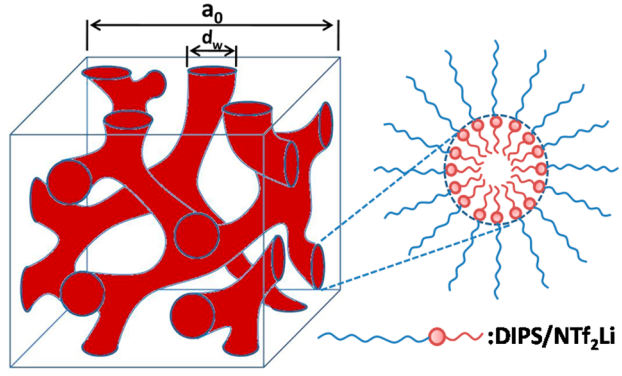


To better understand the lithium-ion conduction mechanism in the system, Arrhenius plots of the ionic conductivity were applied to calculate the activation energies of the systems. The DIPS-$NTf_2Li$ mixture without water has an activation energy Ea=27.76 kJ $mol^{-1}$. The activation energies of the sample with 50 wt % DIPS-$NTf_2Li$ in the $H_1$ phase and the sample with 80 wt % DIPS-$NTf_2Li$ in the $L_\alpha$ phase are 4.41 and 8.10 kJ $mol^{-1}$, respectively. The decrease in activation energies is believed to arise from the change of the conduction mechanism. It is generally accepted that the lithium-ion conduction in the DIPS-$NTf_2Li$ mixture mainly proceeds by the diffusion controlled transport (vehicle) mechanism,[37] whereas in the sample in the $H_1$ phase and the sample in the $L_\alpha$ phase, the conduction is mostly dominated by the hopping (Grotthuss) mechanism, as a

result of their ordered assemblies at the molecular level.[38] Another remarkable fact is that the lithium-ion conduction for the sample with 65 wt % DIPS-$NTf_2Li$ in the $V_1$ phase exhibits even lower activation energy being virtually free from the influence of temperature, which is consistent with our speculation about the influence of the microstructure on efficient lithium-ion conduction.

## CONCLUSION

In summary, we have synthesized a room-temperature IL by mixing imidazolium-type zwitterions with $NTf_2Li$. Based on the aggregation behaviors of this amphiphilic IL, we constructed lithium-ion conductive ILCs having hexagonal, lamellar and bicontinuous cubic structures. The introduction of highly ordered and well-defined LCs structures into DIPS-$NTf_2Li$ IL radically changes the conduction mechanism from diffusion to hopping. Moreover, the formation of the bicontinuous cubic phase further improves the lithium-ion conductivity, and can be of paramount interest for ARLBs applications. We expect this work may indicate the potential of nanostructured aqueous lithium-ion conducting electrolytes in practical applications.

## ASSOCIATED CONTENT

### Supporting Information

The theory for calculation of structural parameters of the liquid crystalline phase. This material is available free of charge via the Internet at http://pubs.acs.org.

## AUTHOR INFORMATION

### Corresponding Author

*E-mail: lqzheng@sdu.edu.cn Phone: +86-531-88361528. Fax: +86-531-8856470.

### Notes

The authors declare no competing financial interest.

## ACKNOWLEDGMENTS

The authors are grateful to the National Basic Research Program (2013CB834505), the National Natural Science Foundation of China (91127017), the Shandong Provincial Natural Science Foundation, China (ZR2012BZ001), and Specialized Research Fund for the Doctoral Program of Higher Education of China (20120131130003).

## REFERENCES

(1) Yang, Z. G.; Zhang, J. L.; Kintner-Meyer, M. C. W.; Lu, X. C.; Choi, D. W.; Lemmon, J. P.; Liu, J. *Chem. Rev.* **2011**, *111*, 3577−3613.
(2) Armand, M.; Tarascon, J. M. *Nature* **2008**, *451*, 652−657.
(3) Li, W.; Dahn, J. R.; Wainwright, D. S. *Science* **1994**, *264*, 1115−1118.
(4) Wang, G. J.; Fu, L. J.; Zhao, N. H.; Yang, L. C.; Wu, Y. P.; Wu, H. Q. *Angew. Chem.* **2007**, *119*, 299−301.
(5) Luo, J. Y.; Xia, Y. Y. *Adv. Funct. Mater.* **2007**, *17*, 3877−3884.
(6) Tang, W.; Liu, L. L.; Zhu, Y. S.; Sun, H.; Wu, Y. P.; Zhu, K. *Energy Environ. Sci.* **2012**, *5*, 6909−6913.
(7) Wang, X. J.; Hou, Y. Y.; Zhu, Y. S.; Wu, Y. P.; Holze, R. *Sci. Rep.* **2013**, *3*, 1401−1405.
(8) Ruffo, R.; Wessells, C.; Huggins, R. A.; Cui, Y. *Electrochem. Commun.* **2009**, *11*, 247−249.
(9) Zheng, J.; Chen, J. J.; Jia, X.; Song, J.; Wang, C.; Zheng, M. S.; Dong, Q. F. *J. Electrochem. Soc.* **2010**, *157*, A702−A706.
(10) Qu, Q. T.; Fu, L. J.; Zhan, X. Y.; Samuelis, D.; Maier, J.; Li, L.; Tian, S.; Li, Z. H.; Wu, Y. P. *Energy Environ. Sci.* **2011**, *4*, 3985−3990.
(11) Wang, Y. G.; Yi, J.; Xia, Y. Y. *Adv. Energy Mater.* **2012**, *2*, 830−840.
(12) Manjunatha, H.; Suresh, G. S.; Venkatesha, T. V. *J. Solid State Electrochem.* **2011**, *15*, 431−445.
(13) Binnemans, K. *Chem. Rev.* **2005**, *105*, 4148−4204.
(14) Xu, F.; Matsumoto, K.; Hagiwara, R. *J. Phys. Chem. B* **2012**, *116*, 10106−10112.
(15) Welton, T. *Chem. Rev.* **1999**, *99*, 2071−2083.
(16) Rogers, R. D.; Seddon, K. R. *Science* **2003**, *302*, 792−793.
(17) Bisoyi, H. K.; Kumar, S. *Chem. Soc. Rev.* **2011**, *40*, 306−319.
(18) Hikmet, R. R. M.; Michels, I. *Adv. Mater.* **2001**, *13*, 338−341.
(19) Kerr, R. L.; Miller, S. A.; Shoemaker, R. K.; Elliott, B. J.; Gin, D. L. *J. Am. Chem. Soc.* **2009**, *131*, 15972−15973.
(20) Yoshio, M.; Mukai, T.; Ohno, H.; Kato, T. *J. Am. Chem. Soc.* **2004**, *126*, 994−995.
(21) Ichikawa, T.; Yoshio, M.; Hamasaki, A.; Mukai, T.; Ohno, H.; Kato, T. *J. Am. Chem. Soc.* **2007**, *129*, 10662−10663.
(22) Ichikawa, T.; Kato, T.; Ohno, H. *J. Am. Chem. Soc.* **2012**, *134*, 11354−11357.
(23) Zhao, M. W.; Gao, Y. A.; Zheng, L. Q. *J. Phys. Chem. B* **2010**, *114*, 11382−11389.
(24) Zhang, S. H.; Yuan, J.; Ma, H. C.; Li, N.; Zheng, L. Q.; Inoue, T. *Colloid Polym. Sci.* **2011**, *289*, 213−218.
(25) Shi, L. J.; Zhao, M. W.; Zheng, L. Q. *RSC Adv.* **2012**, *2*, 11922−11929.
(26) Ueda, S.; Kagimoto, J.; Ichikawa, T.; Kato, T.; Ohno, H. *Adv. Mater.* **2011**, *23*, 3071−3074.
(27) Choi, U. H.; Lee, M.; Wang, S.; Liu, W. J.; Winey, K. I.; Gibson, H. W.; Colby, R. H. *Macromolecules* **2012**, *45*, 3974−3985.
(28) Souza, B. S.; Leopoldino, E. C.; Tondo, D. W.; Dupont, J.; Nome, F. *Langmuir* **2012**, *28*, 833−840.
(29) Fujita, M. Y.; Byrne, N.; Forsyth, M.; MacFarlane, D. R.; Ohno, H. *J. Phys. Chem. B* **2010**, *114*, 16373−16380.
(30) Byrne, N.; Howlett, P. C.; MacFarlane, D. R.; Forsyth, M. *Adv. Mater.* **2005**, *17*, 2497−2501.
(31) Rulkens, R.; Wegner, G.; Albrecht, T. T. *Langmuir* **1999**, *15*, 4022−4025.
(32) Dong, B.; Zhang, J.; Zheng, L. Q.; Wang, S. Q.; Li, X. W.; Inoue, T. *J. Colloid Interface Sci.* **2008**, *319*, 338−343.
(33) Berret, J. F. In *Molecular Gels*; Weiss, R. G., Terech, P., Eds.; Springer: Dordrecht, The Netherlands, 2006; Ch. 19, p 686.
(34) Hato, M.; Yamashita, I.; Kato, T.; Abe, Y. *Langmuir* **2004**, *20*, 11366−11373.
(35) Shimura, H.; Yoshio, M.; Hamasaki, A.; Mukai, T.; Ohno, H.; Kato, T. *Adv. Mater.* **2009**, *21*, 1591−1594.
(36) Hatakeyama, E. S.; Wiesenauer, B. R.; Gabriel, C. J.; Noble, R. D.; Gin, D. L. *Chem. Mater.* **2010**, *22*, 4525−4527.
(37) Kreuer, K. D. *Chem. Mater.* **1996**, *8*, 610−641.
(38) Kreuer, K. D.; Paddison, S. J.; Spohr, E.; Schuster, M. *Chem. Rev.* **2004**, *104*, 4637−4678.